ION INTERACTION WITH SOLIDS: ASTROPHYSICAL APPLICATIONS

E. M. Bringa
Lawrence Livermore National Laboratory
Chemistry and Material Sciences Dir., P.O. Box 808 L-353 Livermore CA 94550 USA
ebringa@llnl.gov

R. E. Johnson
University of Virginia
Engineering Physics Department Charlottesville VA 22903 USA
rej@virginia.edu

Abstract Energetic plasma ions and electrons can significantly alter surfaces in the solar system and the interstellar medium (ISM) and produce observable gas-phase atoms and molecules. In order to understand recent observations, the physics and chemistry of sputtering and radiolysis are reviewed. Emphasis is on recent molecular dynamics simulations of sputtering and their relevance to the desorption of molecules from grains in the ISM by heavy cosmic-ray ions and the effect of energetic ions and electrons on the icy surfaces in the magnetospheres of Jupiter and Saturn.

Keywords: ion bombardment, desorbtion, cosmic rays

1. Introduction

A description of ion-solid interactions is necessary to understand the effects produced by energetic plasma ions and electrons incident on surfaces in the solar system and the interstellar medium (ISM). This interaction can lead to surface charging, sputtering, and to chemical and physical alterations of the exposed surfaces. The materials of interest are refractory, organic and low-temperature condensed-gas solids (ices). In addition to the presence of ices as mantles on grains in the ISM, Table 1 show where"ices" exist in the solar system. It has been shown that these ices are often exposed to and modified by photons and charged particles from the solar wind, planetary magnetospheres and background cosmic rays. Recent Galileo and Hubble Space Telescope data for the Saturnian and Jovian satellites have shown dramatic effects produced by the energetic particles trapped in these planetary magnetospheres.

"Ice"	T_f (K)	Where is it found
water (H_2O)	273 (0)	Earth, Mars, comets, outer planet satellites
carbon dioxide (CO_2)	215 (-58)	Mars, Triton, comets, Callisto
sulfur dioxide (SO_2)	200 (-73)	Io, Europa
ammonia (NH_3)	195 (-78)	Comets, maybe some outer planet satellites
methane (CH_4)	91 (-182)	Triton, Pluto, comets, Kuiper belt objects
ozone (O_3)	80 (-193)	Ganymede, Rhea, Dione
carbon monoxide (CO)	68 (-205)	Triton, Pluto, comets
nitrogen (N_2)	63 (-210)	Triton, Pluto, comets
oxygen (O_2)	55 (-218)	Ganymede, Europa

Table 1. Condensed Volatiles in the Solar System. T_f is the freezing temperature at normal pressure (1 atm) and the value in parentheses indicates the temperature in degrees Celsius. The coldest recorded temperature on Earth was -89 Celsius in Antarctica in 1983. Adapted from W. M. Calvin [1].

A fast ion transfers energy to atoms in a solid by direct momentum transfer to the nuclei or by energy transfer to the electrons. When a swift ion, with velocity greater than the mean speed of outer shell electrons, bombards a solid, a track of electronic excitations is produced along the path of the ion. This is typically referred to as an ion track. By excitations we mean promotion of electrons to excited estates, including ionizations (electron-hole pair formation). Both the momentum transfer collisions and the excitations can lead to ejection of atoms/molecules from the solid, a phenomenon that is called sputtering [2]. Figure 1 shows schematically a sequence of events that lead to sputtering. The sputtering yield, Y, is the number of atoms/molecules that are ejected per individual bombarding ion. When the energy deposited by the ion near the surface is large the surface can be strongly modified with changes in crystallinity and the appearance of craters, rims and hillocks.

Table 2 shows some of the ions that can be found in the interstellar and solar medium.

In the following a brief overview of ion-solid interactions is presented, with emphasis on sputtering processes. First the energy loss and range of ions is discussed, then the formation of the ion track. Several sputtering yield models are discussed, and experimental data are presented. Simulation of ion-solid interactions is shown to be necessary for numerous cases, and the disagreements between analytical models and MD simulations are described. Finally, observations and applications to materials in the ISM and the solar system are described. Readers are strongly

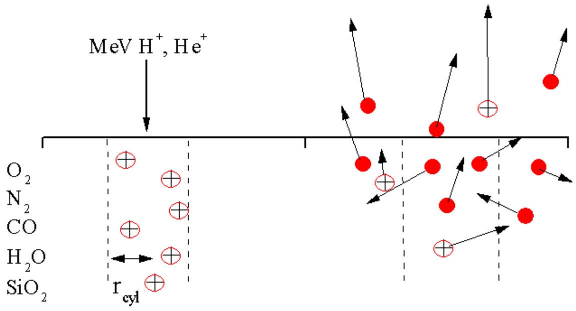

Figure 1. Left frame: The incident ion produces a track of excitations (+ circles); rigth frame, atoms can be ejected from the solid in the ground state (solid circles) or in excited states (encircled +) due to the energy release.

Ions	Energy	Where is it found
H, He	0.5 eV	cometary atmospheres
H, He	1-10 eV	ISM shocks
H,He,...	keV	solar wind
H,O,S,...	keV-MeV	planetary magnetospheres
H,Fe,O, ...	GeV	Cosmic Rays

Table 2. Ions present in the ISM and in the solar system.

encouraged to browse through complementary information on the web, including several movies of the simulations [3] http://dirac.ms.virginia.edu/~emb3t/research/research.html.

2. Stopping Power and Ranges

As a moving ion of velocity $\mathbf{v}$ and energy E traverses a material it experiences a force $\mathbf{F}$ that leads to energy dissipation, $dE/dt = \mathbf{v} \cdot \mathbf{F}$. If x is the direction of motion this can be written as $dE/dt = -(dx/dt)\,F$. The energy loss per unit path length, also called the "instantaneous" stopping power of the ion, is given by $dE/dx = F$. There are entire books [4] and reviews [5] dedicated to the stopping power. The stopping of low velocity ions was studied by Firsov [6], and Linhard and coworkers developed an electronic stopping model at low velocities based on the Thomas-Fermi approximation [7]. The dielectric ("linear") formalism for electronic stopping [8, 9] is widely used but it has many limitations [10]. Monte Carlo techniques employed in combination with the Binary Collision approximation have been used since 1963 [11]. Ziegler, Biersack and Littmark developed a 'universal' potential (ZBL) for use in Monte Carlo models of stopping in 1985 [4].

Typically, it is assumed that the stopping power can be separated into several components according to the physics of the energy loss processes:

$$(dE/dx) \approx (dE/dx)_n + (dE/dx)_e \quad (1)$$

$$(dE/dx)_e \approx (dE/dx)_{excit.} + (dE/dx)_{charge-exch.} + (dE/dx)_{ioniz.} \quad (2)$$

These are the elastic collision (momentum transfer to nuclei), $(dE/dx)_n$, and electronic contributions, $(dE/dx)_e$. These can be further broken down as indicated above. Although used by everyone for convenience, this separation is only approximate since the momentum transfer and electronic processes are correlated. For scaling purposes, (dE/dx) is often given as a function of the dimensionless energy,
$\epsilon = M_T E_P \, a / \left[(M_T + M_P) \, Z_P Z_T e^2 \right]$, which depends on the projectile energy E_P, projectile and target mass $M_{P/T}$, charge $Z_{P/T}$, and screening length a. Nuclear stopping dominates for $\epsilon \leqslant 10$, and the electronic stopping dominates for $\epsilon \gtrsim 100$. At low velocities both nuclear and electronic stopping are roughly proportional to $\sqrt{E_P}$. They then reach a maximum [at $\epsilon \approx 0.5$ for $(dE/dx)_n$ and at $\epsilon \approx 100$ for $(dE/dx)_e$], and at high velocities, they decay as $(\ln E_P)/E_P$ (for non-relativistic ions). The stopping of water is shown in Fig. 2.

Once the stopping power is known the range of the projectile within the material is calculated as:

$$R = \int_0^{E_o} |dE/dx|^{-1} \, dE \quad (3)$$

The energy deposition versus depth for a high velocity projectile is roughly constant except at the end of the particle's path, where it increases significantly (Bragg's peak). Since the range of 1 MeV He^+ in solid O_2 is 6 μm it is reasonable to consider the energy deposition to be constant along the cylindrical track, as pointed out in Section 2.1. On the other hand, the range of a 10 keV C ion in carbon is only 240 Å and one has to take into account variations in the energy deposition with depth.

There are two main limitations in models for stopping power. First, all analytical and semi-analytical models of stopping deal with monoatomic materials. In order to calculate the stopping power of a multicomponent solid, corrections have to be made. The Bragg rule and bonding corrections [4, 12] can be applied but their success is limited. Second, the

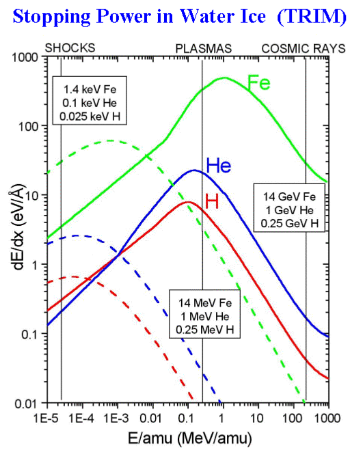

Figure 2. Stopping power of H, He and Fe in water, obtained from TRIM. $(dE/dx)_n$ (dashed lines) and $(dE/dx)_e$ (solid lines).

energy deposited near the surface is different from the value measured at depth, called the equilibrium stopping power, even if the velocity remains almost constant. Often the energy deposited near the surface, which controls sputtering, is given as a fraction [13, 14] of the stopping power inside the solid, which is the tabulated value, $(dE/dx)_{surf} = \alpha\,(dE/dx)$.

For the $(dE/dx)_e$ component, some of the excited atoms and molecules decay producing photons and chemical rearrangements and do not contribute to the sputtering. Therefore, only a fraction, f , of $(dE/dx)_{surf}$ is relevant [14]. In this way, the effective stopping power contributing to sputtering by the electronic energy deposition is given by:

$$(dE/dx)_{eff} = f\,(dE/dx)_{surf} = f\alpha\,(dE/dx) = \eta\,(dE/dx)\,. \qquad (4)$$

The value of η varies for different combinations of projectile and target properties. For MeV He^+ bombarding solid O_2, α was calculated to be ~ 0.4, and $f \sim 0.5$ was obtained by fitting the sputtering data, giving $\eta \sim 0.2$ [14] . For keV protons bombarding O_2, η is roughly 0.5 [14].For many astrophysics applications we are primarily interested in atomic ion projectiles in the regime beyond the maximum in the electronic stopping power. Here the nuclear contribution is negligible and charge exchange can be neglected, leaving excitations and ionizations as the main contribution to the stopping power.

3. Ion Tracks

When energetic electrons, photons or ions bombard a solid they produce a number of excitations (including ionizations) along their path through the material. A fast ion typically creates a track of excitations along its path. In this track the excitation density depends on the incident ion energy and the target material. Fast electrons (velocity $> 2v_o$, with v_o the Bohr velocity) either directly incident or from an ionization produced by an energetic photon or an ion will, on the average, produce an additional ionization at some distance from the track. These electrons suffer significant angular scattering and produce a number of events near the end of their track, a region often called a 'spur' in which multiple ionizations are produced in a small volume.

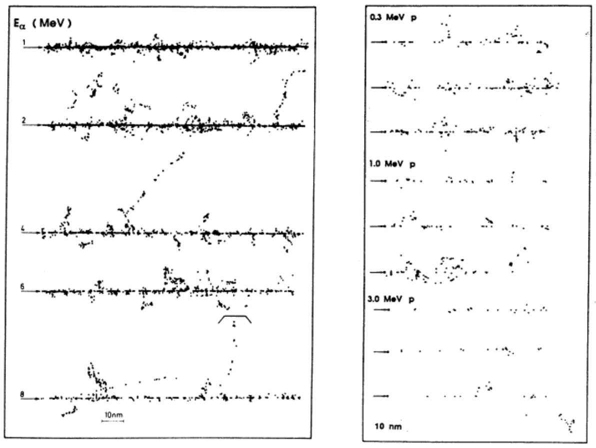

(a) (b)

Figure 3. (a) α particle tracks (1, 2, 4, 6 and 8 MeV) in water. (b) Proton tracks (0.3, 1.0 and 3.0 MeV) in water. All tracks calculated with the Monte Carlo code MOCA-14, from Paretzke *et al.* [16]. Notice that the He tracks are nearly continuous, and that there are significant statistical variations for the same energy for proton tracks.

We have been mainly interested in ions that penetrate a solid without large deflections creating a nearly cylindrical track of excitations. This is the case for swift light ions, such as H^+ or He^+, penetrating condensed gas solids. As can be seen for MeV α particle tracks in water in Fig. 3 (a), typically more than one excitation per monolayer is produced, corresponding to what we refer to as the high excitation density regime.

The maximum of the electronic stopping power for protons in water is at $\sim$100 keV (Fig. 2). The stopping power decreases as energy increases in Fig. 3 (b) and it is seen that the probability of excitation also decreases leading to a sparse track. The transition from dilute excitations produced by medium energy protons to a high density of excitations for MeV He^+ has been studied for atomic targets [15]. Although we usually consider average quantities, like dE/dx, the tracks have large statistical fluctuations in excitation density. For a given energy, two tracks can have very different excitation distributions, as can be seen in Fig. 3 (b) for proton tracks in water in which excitations are sparse. This is important when describing the effect of cosmic-ray ions on grains.

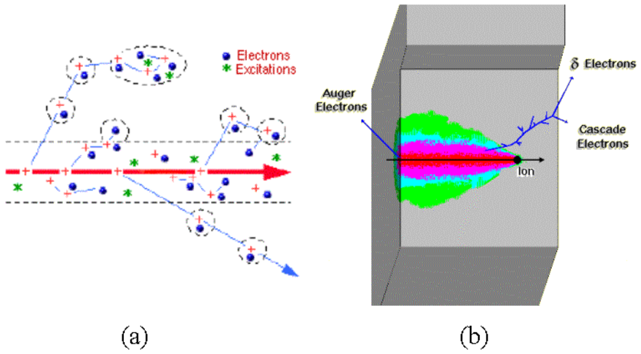

Figure 4. Tracks produced by a heavy ion. (a) The infratrack is marked with dashed lines. (b) Track structure showing secondary electrons. Colors indicate the strength of the track potential felt by the electrons (darker indicates higher value).

A schematic view of the track of excitations produced by a fast ion can be seen in figure 4 (a). There are primary excitations produced directly by the ion and secondary excitations produced after the passage of the ion by energetic secondary electrons and by excited state diffusion. The region in which the primary excitations are produced is often called the infratrack. The size of the infratrack is equal to a lattice spacing at low velocities, but at high velocities is given roughly by the Bohr adiabatic radius [16, 17], $r_B = \pi v/\omega$, where the excitation energy is $\hbar\omega$.

In the infratrack an energetic incident ion produces Auger electrons, low energy secondary electrons ($\lesssim 10$ eV), and more energetic electrons often called δ rays. The range of these δ electrons can be quite large ($\sim$100 Å) and determines an outer limit to the track in the absence of exciton diffusion. This region of excitation determined by the δ electrons is often called the ultratrack [16, 17]. The size of the ultratrack is proportional to the energy of the incident ion and the spurs (or "blobs") are enclosed by dashed spheres or ellipses in Fig. 3(a). As the ion slows down the energy of the δ electrons decreases giving rise to the conical ultratrack seen in Fig. 4 (b). For surface modification and sputtering phenomena the energy deposited near the surface is important. In cases where $Y \sim 1$, the first 2-3 layers typically control sputtering, but for much larger yields energy deposition from deeper layers participates. Therefore, even when the ion penetration is not large, the conical shape of the ultra-track can often be neglected and considered roughly cylindrical.

Energy relaxation in the solid is a complex process involving several possible pathways in which the excitation energy is released to the lattice. This is shown in Table 3 for a solid with atoms "A". Repulsive states lead to extra kinetic energy (ΔE) deposited in the lattice which can cause sputtering and surface modification. The complexity of the relaxation process increases for molecular solids or multicomponent solids in which chemical reactions can occur.

Coulomb Repulsion	$A^+ + A^+ \rightarrow A^+ + A^+ + \Delta E$
Charge Exchange	$A^{++} + A \rightarrow A^+ + A^+$
De-Excitation	$A^{**} + e \rightarrow A^* + e(hot) \rightarrow A^* + e + \Delta E$
Repulsive Decay	$(AA)^* \rightarrow A + A + \Delta E$
Lattice Relaxation	$A^{**} + \text{lattice} \rightarrow A^* + \text{lattice} + \Delta E$
Dielectronic Recombination	$A^+ + e + e \rightarrow A^* + e(hot) \rightarrow A^* + e + \Delta E$

Table 3. Track processes.

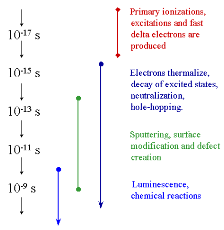

Figure 5. Timeline of the events produced by the bombarding ion.

A time line for the track processes in the physical stage is given in Fig. 5. Early track evolution is relatively well understood [16, 18] as is the other extreme, chemical effect in times of the order of μs or longer [19]. However, events occurring on the scale of ps, including the coupling of electronic excitations to the lattice, are not easily calculated [20]. In the next section models and data for sputtering and surface modification are described.

4. Sputtering

Three different regimes can be found for the collisional sputtering process. The single knock-on regime occurs when a primary recoil receives enough energy to be ejected. In the linear collision cascade (LCC) regime a number of recoils can lead to sputtering and collisions occur mainly between fast atoms and atoms at rest. When many atoms within the "cascade" volume are moving, collisions among moving atoms can not be neglected and the LCC model breaks down [21, 14, 23, 24, 25]. This is the "non-linear" or "spike" regime, for which there is, at present, no standard way to evaluate the sputtering yield or the angular and energy dependence of ejecta. Thermal spike models, which were used to describe the sputtering of refractory (binding energy of few eVs) materials have also been used to parametrize measured yields from low-temperature ices like O_2 and N_2. Recently we showed that the standard analytic models were incorrect in the nonlinear sputtering regime [15]. Below, the LCC model and the thermal spike models are summarized.

4.1 Linear Collision Cascade (LCC) Sputtering

The work by Sigmund [13] has lead to a standard analytic model for estimating the sputtering yield for amorphous and polycrystalline materials in the nuclear dE/dx regime at low energy densities. When the solid is a single crystal the experimental yield varies for different crystalline orientations of the target. Phenomena like channeling and collisions along a crystalline axis appear and the LCC model can be applied with certain modifications.

In the LCC, the yield for an amorphous solid is typically obtained by assuming binary collisions and obtaining the recoil spectra. The result from which most of the properties evolve is the spectrum of recoils set in motion with energy between E' and $E' + dE'$. This varies roughly as $[dE' \,/\, E'^{\,2}]$ with only a weak dependence on the form of the interaction potential between the atoms. However, the binary collision assumption in the LCC model is not necessary as this energy spectrum also applies to low energy recoils and collisions involving molecules [26]. The form for the yield has been derived often

$$Y \approx C\ (l/U)\ (dE/dx)_n \tag{5}$$

$$(dY/d\theta)\ /Y \approx (\cos\theta)^{-1} \tag{6}$$

$$\begin{aligned}(dY/d\Theta)\,/Y &\approx (\cos\Theta)^{-b} &(7)\\ (dY/dE)\,/Y &\approx \frac{2UE}{(E+U)^3} &(8)\end{aligned}$$

Here U is the surface binding energy, Θ is the angle to the surface normal, θ is the ejection angle measured from the surface normal, E is the energy of the an ejected atom, and C is a parameter that depends on the interaction potential and projectile-target parameters. The yield in the LCC regime is seen to be proportional to the energy deposited in the surface region and inversely proportional to the binding energy U. Sigmund [13] estimated the parameters using the first few moments of the transport equation for the recoils. He wrote $C\ (l/U) = \Lambda\alpha$ where Λ depends only on target properties such as U and α depends the mass ratio M_T/M_P and weakly on the electronic energy loss and the interaction potential. $\alpha\,(dE/dx)_n$ gives the energy deposited at the surface, as discussed, and is sometimes written as $F_D\,(0)$. LCC fits the energy dependence of the experimental data in the regime at low $(dE/dx)_n$ but the parameter α, adjusted to fit the magnitude of the data, agrees with the model values to about 50%.

The angular distribution of the ejecta in Eq. 6 was assumed to be $\cos\theta$ for a flat surface, although this form is not found experimentally or in detailed calculations. The change of the yield for different angles of incidence of the projectile with respect to the surface normal, Θ, was estimated for not-too-oblique incident angles using $b \sim 5/3$ for $M_T/M_P \lesssim 3$ and $b \sim 1$ for $M_T/M_P > 8$. At large angles the yield decreases abruptly due to projectile scattering and surface roughness.

The energy spectrum of the ejecta in Eq. 8, called the Thompson spectrum [27], is obtained assuming a planar binding energy and the recoil spectrum $\propto E'^{-2}$. This can change slightly according to the interaction potential among the target atoms and due to emission from deep layers [28]. The Thompson distribution has a maximum located at $U/2$ and roughly applies up to the maximum possible energy of a primary recoil.

4.2 Sputtering Models in the Non-Linear Regime

In the nuclear stopping (elastic collision) regime, the cascade of collisions directly generates a hot region, a “spike”, that leads to ejection. In the electronic stopping regime, the mechanism for converting electronic energy into lattice motion can be either the transfer of energy to the lattice by the secondary electrons [29, 30] or by a repulsion process because the electrons do not fully screen the nuclear charge. The repulsion may occur on electronic recombination ($O_2^+ + e \rightarrow$ repulsive state $\rightarrow$ O+O+ΔE), by a net repulsive force in the track, or by the short lived, partially screened Coulomb force [31]. Once the energy is in the lattice motion, due either to electronic or collisional processes, then the spike models (thermal spikes, shock models, etc.) can be applied to treat the evolution of the energy and to calculate sputtering.

4.2.1 Analytical Spike Models for Sputtering.

A dense collision cascade is often described as a "spike" and analytical models have been applied to defect production and track formation [29], ion-beam mixing [32], cratering [33], and sputtering of metals and insulators [34]. The sputtering yield is obtained by calculating the temperature profile at the surface and evaluating the yield as:

$$Y = \int_0^\infty dt \int dA \; \Phi \left(T_{surf}, U_s\right) \tag{9}$$

where the integral is over time, t, and surface area, A. Here Φ is the evaporative flux which depends on the surface temperature T_{surf} and binding energy U_s. When the yields are large the cohesive energy (sublimation energy), U, is generally used for U_s and in most cases $T_{surf} \approx T_{bulk}$ is also assumed. Models dealing with spherically symmetric spikes [34] are often appropriate for very low energy ions in the nuclear stopping regime. Below we focus on cylindrical spikes produced by a fast ion.

The formula for the evaporation flux is often taken to be that for a hot gas,

$$\Phi\left(T\right) = n\sqrt{\frac{k_B T}{2\pi m}} \exp\left(-\frac{U_s}{k_B T}\right); \tag{10}$$

Assuming that ejection occurs at some average effective temperature T_{eff} from a region of radius R_{sput}, for a time t_{sput}, then Eq. 9 can be approximated as:

$$Y \approx \pi R_{sput}^2 t_{sput} \Phi\left(T_{eff}, U\right) = n\pi R_{sput}^2 t_{sput} \sqrt{\frac{k_B T_{eff}}{2\pi m}} \exp\left(-\frac{U_s}{k_B T_{eff}}\right) \tag{11}$$

Such a model also results in a Maxwellian energy distribution for the ejecta, which has been seen in some experiments [25] and applies roughly at relatively low dE/dx. In general, T will vary during sputtering and ejection will be largest at the center of the track.

For a narrow, high (dE/dx) spike it has been shown that Eq. 9 gives a yield of the form,.

$$Y \propto (dE/dx)^2_{eff} \tag{12}$$

Eq. 12 is a very robust result verified by analytic and numerical [35, 36] models. The corresponding energy spectrum, $(dY/dE)/Y$, has less steep dependence at large E than in Eq. 8. Since ejection is assumed to be driven by evaporation, an isotropic $\cos\theta$ angular spectrum of ejecta applies. For a narrow track [70, 37] the incident angle dependence is $\sim (\cos\Theta)^{-1.68}$, with a steeper dependence at low dE/dx and large track radii [38].

A large spike temperature at high excitation density can cause an increased pressure in the track, an effect neglected in most thermal spike models. There are also models in which thermal diffusion is assumed to be smaller effect than the large pressure buildup. In such models the yield is estimated from the pressure or shock wave formed. This has been applied to sputtering of macromolecules, like amino acids, for which the yield respect to dE/dx appears to be roughly cubic instead of quadratic [39] and has been suggested to be important in the ISM [40]. Details about pressure effects can be found elsewhere [41].

4.2.2 Computer Simulation Models for Ion-Solid Interaction. Computer simulation methods for ion-solid interactions are described in a number of texts [42, 43] and in a number of reviews [44, 45]. There are three main groups of models: hydrodynamic models, MD models and the Monte Carlo binary collision (BCA) models mentioned earlier. The latter can only be used in the LCC regime and the first can only be used in the non-linear regime. MD can be used to cover the full range and has been applied to sputtering since the early work of Harrison and coworkers [46]. BCA Monte Carlo codes, like TRIM [12] , can only be applied to amorphous materials, whereas MARLOWE [47] is for an ordered target. MD and BCA codes agree reasonably well for amorphous targets and recoil energies much larger than the binding energy of the crystal. For crystalline targets and low primary energies ($E \leqslant 15U$) Monte Carlo codes fail [48]. MD codes are especially suited to study non-linear sputtering and sputtering of molecular solids, crystalline alloys, and effects related to low energy recoils.

5. Molecular Dynamics (MD)

Molecular Dynamics (MD) is a simulation technique widely used to deal with many-body problems and there are several good texts which contain Fortran or C codes. [49, 50]. A monograph can be downloaded from the web [51] giving a good overview of simulation potentials. MD simulations give insights into material behavior at small dimensions and times which are inaccessible experimentally. The main advantage of MD over Monte Carlo is that it provides true dynamical information on the system, because one solves the equations of motion and does not just advance the system based on transition probabilities. A collection of useful MD-related bookmarks can be found in the web at http://dirac.ms.virginia.edu/∼emb3t/Public/MDbook.html.

In this section bold symbols represent vectors, while italics represent scalars. For instance, the distance between two points $\mathbf{r}_i$ and $\mathbf{r}_j$ is given by $r_{ij} = |\mathbf{r}_i - \mathbf{r}_j|$. Classical MD consists in solving Newton's Equations of motion for a collection of N particles with positions $\mathbf{r}_i$ (where $\mathbf{r}_i$ is a 3D vector) and with a potential energy function ϕ, giving $3N$ coupled second order differential equations:

$$m_i \ddot{\mathbf{r}}_i = \mathbf{F}_i = -\nabla_{\mathbf{r}_i}\phi \qquad i = 1, .., N \tag{13}$$

The above set of equations is equivalent to solving $6N$ first order differential equations for both the positions and the momenta $\mathbf{p}_i$:

$$\begin{aligned} \dot{\mathbf{r}}_i &= \mathbf{p}_i/m_i \\ \dot{\mathbf{p}}_i &= -\nabla_{\mathbf{r}_i}\phi \end{aligned} \tag{14}$$

Classical forces can be used when the wavelength of moving atoms, $\lambda = \sqrt{2\pi\hbar^2/Mk_BT}$, is shorter than the mean particle distance, $l = n^{-1/3}$, where n is the number density in the material. The zero point energy of crystals can be roughly incorporated into the classical simulation but the discreteness of energy levels poses a problem at low local temperatures in the simulation of vibrational and rotational excitation of molecules and clusters.

The collisional energy transfer regime can be directly simulated by bombarding a sample with the ion and choosing appropriate interaction potentials. In the electronic regime, an energetic, non-radiative repulsive decay may be represented by giving an atom or neighboring atoms in the lattice an extra kinetic energy, $\Delta E \approx E_{exc}$, such that the total extra energy per unit length is equal to $(dE/dx)_{eff}$. In reality, excitation relaxation processes are more complex but can be described accurately if necessary [52].

MD has several limitations regarding the size of samples and simulation times. To calculate the evolution of a weakly bound L-J solid with a $\sim$0.5 μm side (4 10^9 atoms) for 20 ns (10^6 steps for a typical time step of 0.02 ps) even the most optimized MD codes have calculation times of 0.5 μs/atom/step/CPU. Therefore, it would take 63 years on a single CPU, assuming it has enough memory! If the code is running in parallel using

100% of CPU time in 1000 CPU's it would still take 23 days, neglecting overhead due to communications. Currently most MD simulations are used for relatively small volumes ($\sim 10^5$ atoms) and short times (~ 10 ps). They can then be combined with MC or continuum codes to expand the time and length scales [53, 54, 55].

5.0.3 Analytic spike models versus MD simulations. MD simulations of cylindrical spikes show that analytic models work reasonably well for energy densities $(dE/dx)_{eff}\ /\pi r_{cyl}^2$ that are much less than the cohesive energy density nU, but fail at high energy densities [15]. If these models are corrected by solving the full set of hydrodynamic (HD) equations using realistic transport properties and allowing for flow toward the surface as well as radial flow, the results agree reasonably well with MD, with some discrepancies because escape from the surface is not easily included [41]. Below we parametrized the MD results for the sputtering yield at high $(dE/dx)_{eff}$:

$$Y \approx C\,(r_{cyl}/l)^x \left[(l/U)\,(dE/dx)_{eff}\right]^y, \quad [(dE/dx)_{eff}\ /\pi\, r_{cyl}^2] > nU\,?? \tag{15}$$

For atomic solids $C \approx 0.14$, $x = 0.9 \pm 0.2$, and $y = 1.1 \pm 0.2$. For solid O_2 ([14]) $C \approx 0.092$, $x = 1.0 \pm 0.3$, and $y = 1.0 \pm 0.2$.

6. Experimental data on sputtering and surface modification

There are many experiments on sputtering by ion bombardment and results differ greatly depending on the nature of the material. However, two broad regimes can be identified. One in which the number of excitations or collisional energy transfer events is small but are sufficiently energetic to cause sputtering independently (dilute excitations, typically low dE/dx). This results in a yield that is linear in dE/dx. The other regime occurs when excitations can not be assumed to act independently (either low energy events and low sputtering yields or a high density of excitations at high dE/dx) giving a yield which depends non-linearly on dE/dx. These regimes, discussed below, apply when either collisional and electronic energy deposition dominate.

Electronic sputtering is significant in relatively few materials because the energy release in an event is generally of the order of the binding energy of many materials (few eVs). Although electronic energy deposition can lead to defects, amorphization, desorption of adsorbed species, and radiolytic decomposition, bulk atom ejection is problematic. Therefore, unless the electronic excitation density is extremely large sputtering of bulk refractory material is produced mainly by collisional energy deposition. This is often smaller than electronic energy deposition, but high energy recoils are produced by a single collision event. Electronic sputtering yields are large principally for the condensed gas solids, which have low binding energies (0.5 eV for water; 0.32 eV for SO_2; ~0.08 eV for O_2, N_2 and Ar; and ~0.01 eV for H_2 and D_2) [2], but are also non-negligible for organic solids, relevant in many regions of space, and ejection of the most volatile radiolytic decomposition products such as oxygen and alkalis [56].

6.1 Dilute excitations

6.1.1 Collisional Regime. A large portion of available sputtering data for refractory solids falls into the dilute regime [57]. Programs like TRIM [12] and MARLOWE [47] give reasonable agreement with experiments, especially when the surface binding energy in the code is adjusted to fit the data. For heavy ions the experimental results depart from the LCC model at high dE/dx.

6.1.2 Electronic Regime. When excitations act independently, the energy release by non-radiative decay of individual excitations in a material with a very low U can lead directly to desorption or can initiate a mini-cascade below the surface giving a yield roughly linear in $(dE/dx)_e$. This happens for three different cases: 1. When the mean free path for producing excitations λ_{exc} is large compared with the mean lattice spacing $l = n^{-1/3}$ where $\lambda_{exc} = W/(dE/dx)$, and W is the average energy required to produce an excitation [15]; 2. The excitations are initially close together but exciton diffusion is rapid so the non-radiative decay events are again spatially dilute [2]; 3. Excitations decay over long times (up to μs) and are well separated temporally.

6.2 High excitation density

In this regime the excitation density is important. For electronic sputtering of the molecular condensed gas solids, this occurs for excitation densities ranging from ~1 to several per monolayer. The energy from the closely-spaced individual decay events can create a hot track where moving particles collide with other moving particles or the closely-spaced excitations overlap creating a more robust release of energy. Also, when the density of electron-hole pairs is large enough and the electronic screening and recombination are small enough "Coulomb explosion" can heat the lattice [31]. In these cases a region in which the local temperature is much higher than the temperature of the rest of the solid is produced. It can be higher than the melting temperature and even higher than the binding energy of the solid. Coulomb explosion was first proposed for track formation in insulators [58]. Tracks have been seen to be produced by solar flare helium ions in lunar grains and collected interplanetary grains. With the advent of new accelerators tracks can be produced even by electronic excitation of metals at enormous $(dE/dx)_{elec}$ (tens of keV/Å) [59].

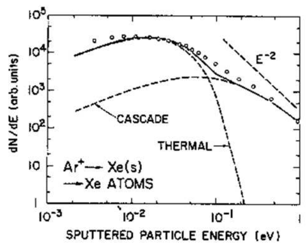

Figure 6. 3 keV Ar bombardment of polycristalline Xe, at incident angle $\Theta = 60^o$, from Kelly [60]. Cascade+ thermal contributions. Cascade spectrum uses $U = 0.16$ eV and thermal spectrum uses $T = 200$ K.

At high excitation density the dependence of the yield on dE/dx in both the nuclear stopping regime and electronic stopping regime is similar because the high temperature spike evolves similarly. A "typical" energy spectra of the ejected particles for high energy densities [60] can be seen in Fig. 6. The spectrum labeled as thermal is the one from Urbassek and Michl [23]. The maxima in the spectrum is shifted towards lower ejecta energies than is the case for LCC. Measured energy distributions are often fit using a Thompson distribution [27] with an artificial U [61, 62]. That is, the process can still exhibit the cascade energy spectrum ($\sim 1/E^2$) but with a lower effective U because of surface damage [46]. However, the shift of the maximum can also be due to late evaporative contributions. In Fig.6, a Thomson spectrum does not fit the data well. Therefore, a realistic model must include the weakened binding in the track region [24] and late thermal effects [63]. The energy distribution is usually measured at a fixed angle and can differ from the angular-integrated distribution, leading to apparent shifts in the binding energy. The fact that the distribution often goes as E^{-2} at large E is general, as it is determined by the energy partition among the recoils

[26] so that E^{-2}-like tails are also observed in the "non-linear" regime [63, 36, 15].

6.2.1 Collisional Regime. The transition from linear to non-linear regime occurs when the energy density in the cascade volume is of the order of the binding energy per atom, in which case sputtering yields are ∼10-20. Enhancements, which are underestimated by LCC, are also produced by impact of ion clusters. Therefore, spike models have been applied to cluster ion sputtering of metals [21]. Heavy atomic projectiles [63] and cluster ion impact [64] can produce a hot region with a transient fluid at the center. Nuclear sputtering of condensed gas solids has been studied experimentally [65] and the transition from the LCC to the nonlinear regime has been described for one case [66].

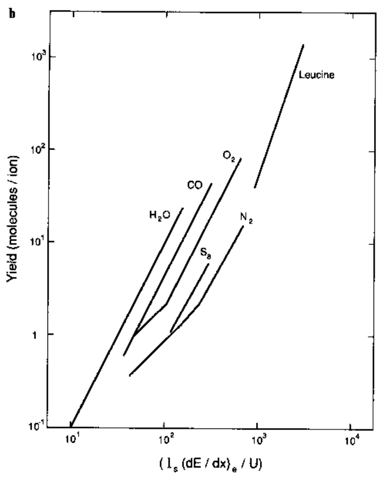

Figure 7. Experimental sputtering yields as a function of dE/dx, scaled with the binding energy U and the mean particle distance l, for several condensed gases [2].

6.2.2 Electronic Excitations Regime. In Fig. 7 it is seen that the sputtering for a number of low cohesive energy, condensed gas solids (O_2, N_2, CO and H_2O) is roughly quadratic in dE/dx at high excitation densities (high dE/dx). For the range of dE/dx shown, water ice does not exhibit the linear regime. This has only been observed at very low dE/dx using ∼100 keV electrons [67]. The yield for the amino acid leucine is also included in the figure. Over a narrow range of dE/dx it appears to be steeper, possibly cubic [39].

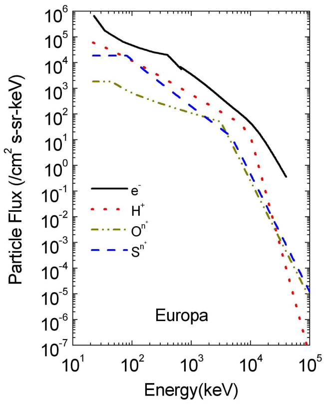

Figure 8. Particle fluxes on Europa, derived from Galileo data.

A linear regime is observed in solid O_2. A single electronic recombination event decays as follows: $O_2^+ + e \rightarrow$O+O+ΔE [2] with energy release, $\Delta E \approx 1 - 10$ eV shared between the atoms. Since $U \approx 0.08eV$, a single excitation can lead to sputtering. However, in water ice, $H_2O^+ + e \rightarrow$H+OH+ΔE or H_2+O+ΔE or H_2O^++$H_2O$$\rightarrow$$H_3O^+$+OH, and $H_3O^+ + e \rightarrow H_2$+OH+$\Delta E$. Since $\Delta E \approx 1 - 5$ eV and the binding energy is much higher, $U \approx 0.5$ eV sputtering due to an individual excitation event is problematic. This is especially so since the lightest species carry off most of the energy resulting in hot H and H_2 that are seen in experiments [68]. For weakly attached adsorbed water molecules other ejection processes are possible.

The energy spectra for heavy water (D_2O) ice from Brown et al. [61] for 50 keV Ar^+ the Thompson spectrum agrees well with the experiment if the effective binding energy is approximately ten times smaller than the binding energy of water (~ 0.5 eV). When $(dE/dx)_{el}$ dominates[1], the low energy component grows, again suggestive of spike effects [62]. As mentioned before, "Coulomb explosion" may contribute. At both low and high $(dE/dx)_e$ sputtering by this process varies as $(dJ/dx)^2$, where

[1] 1.5 MeV He^+ in liquid water has $(dE/dx)_{el} = 18.2$ eV/A, $(dE/dx)_{nuc} = 0.02$ eV/A, and a penetration depth of 8.4 μm. 1.5 MeV Ar^+ in liquid water has $(dE/dx)_{el} = 83.5$ eV/A, $(dE/dx)_{nuc} = 7.4$ eV/A, and a penetration depth of 2.4 μm. 50 keV Ar^+ in liquid water has $(dE/dx)_{el} = 13.8$ eV/A, $(dE/dx)_{nuc} = 37.4$ eV/A, and a penetration depth of 10^{-1} μm. These values were calculated for liquid H_2O using SRIM 98 [12].

dJ/dx is the ionization per unit path length [31] and, therefore, may be important in the sputtering of ice.

The yield is seen to increase with increasing angle to the normal, Θ. This occurs due to the increase of energy deposited near the surface up to a point ($\Theta \geq 60^o$) where projectile backscattering and surface roughness affect the yield. Angular data for sputtering of solid CO, O_2 and other condensed gas solids [69, 70] can be well approximated as $Y(\Theta) = Y(0)(\cos\Theta)^{-1.6}$. MD simulations of ejection from a hot track also give the same dependence [71]. Coincidentally, a thermal spike model for constant thermal diffusivity and narrow spike radius gives the same dependence at small angles [37].

6.3 Chemical Effects

Incident particles and energetic photons not only cause sputtering but can also cause chemical alteration of the solid, a process called radiolysis or photolysis [72]. Therefore, even in a pure material a number of newly formed species can be ejected. The dominant ejecta are typically those with the lowest surface binding energy. For this reason ions, that have a strong attraction to the surface, are sputtered inefficiently even though they are studied most frequently as they are easy to detect. Radicals formed in repulsive decays can be ejected from the surface layer more easily than ions and can be an important component at low yields. Because their binding energies are still large, they have, typically, much lower yields than any close shell atoms or molecules that can be produced. Because the surface binding acts as a filter, the sputtering of ice by energetic ions is typically dominated by H_2O, H_2 and O_2 with the latter becoming increasingly important with increasing temperature. Although the O_2 is not produced as efficiently as the radicals OH and H, it is very weakly bound to the solid and can diffuse along the ion track to the surface. Similarly, the sputtering of CO_2 and CO are both dominated by CO, O_2 and CO_2 with more refractory products such as carbon suboxides (C_xO_y) accumulating in the irradiated sample. In solid oxygen the dissociation of O_2 leads to the formation of ozone, which it self is readily dissociated releasing energy to the lattice [73].

Because the chemistry induced by energetic ions is qualitatively similar in most instances to that induced by photons and discussed extensively at this conference, it will be only touched on here. As in a space environment, irradiation in the presence of a vacuum interface will lead to the loss of the most volatile species (e.g., Na and K from most minerals, O_2 from a silicate, H_2 from water ice) and the most refractory species formed will accumulate (e.g., carbon chains in organic solids). In addition, segregation will occur under long term irradiation and defects will accumulate to form voids (interior surfaces). Radiation yields are often given as a G-value, the number of a particular radiation product per 100 eV deposited in the solid. Unfortunately, G-values vary slowly with ion energy and type and material temperature as they are affected by the local energy density.

7. Applications: Planetary

One of the most exciting areas of research in Planetary Science is the study of the sputtering and the chemistry induced in the surfaces of the icy moons of Jupiter and Saturn by the Jovian and Saturnian magnetospheric particle radiation. Observations of Io, Europa, Ganymede and Callisto by Galileo using the newly discovered telescope initiated enormous controversy and changed our image of the solar system over three centuries ago. Now observations of these moons using the instruments on the Galileo spacecraft and Hubble Space Telescope (HST) are again leading to radically new ideas on the origins of bodies in our solar system and, possibly, to new insights into the origins of biological activity. Objects in Saturn's magnetosphere are now being studied using HST and our understanding is also expected to grow dramatically when the CASSINI spacecraft arrives at Saturn in 2004.

7.1 Sputtering of the Icy Galilean Satellites

The new spacecraft and HST observations satellites require an understanding of the changes induced in the surfaces of the Galilean satellites by the energetic ions and electrons trapped in the giant magnetosphere of Jupiter [74]. These energetic particles both alter the material and cause desorption of atoms and molecules, producing a tenuous atmosphere and ionosphere. Whereas the dominant surface material on the outer three Galilean moons is ice (Table 1), the inner moon, Io, is the most active volcanic object in the solar system. It has been totally dehydrated and has a surface coated in sulfur dioxide.

Also remarkable is the fact that one of the icy moons, Ganymede [76], has an intrinsic field and all of the icy moons have unusual conducting properties as indicated by the magnetometer measurements on the Galileo spacecraft. This has been attributed to the presence of underground, tidally heated oceans [75]. The magnitude of the conductivity deduced from the time variability of the local fields suggests the presence of underground 'salty' oceans. Supporting this hypothesis, the surface of Europa is chaotic with geologically young material on the surface. Recent infrared spectra are indicative of hydrated salts and organics [77], which would be consistent with material from an underground ocean. For this reason Europa is now considered to be an object on which biological materials might have evolved. Such an evolution, if it occurred, could be driven by the heat created by the tidal interaction with Jupiter or it could be driven by the energy of the Jovian magnetospheric particle radiation incident on to the surface [88]. A recent laboratory comparison of the shape of the water of hydration bands with the spectra obtained by the Galileo spacecraft suggests that the hydrated material might be frozen, hydrated H_2SO_4[89]. This material would be produced by the charged particle irradiation of sulfate salts, sulfur or SO_2 in an ice matrix [81] so that a sulfur cycle is maintained by the incident radiation. Such activity produces oxidants such as SO_4^{-2} , H_2O_2 and O_2 which have potential importance for pre-biotic chemistry.

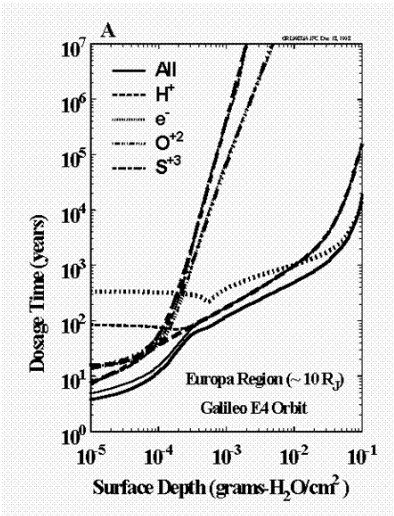

Figure 9. Time required to achieve a dose of 100 eV/molecule in water ice.

Using the data from the Energetic Particle Detector on the Galileo spacecraft, the ion and electron fluxes are given in Fig. 8. In addition, a lower energy component exists [90]. Since the dominant volatile species on the Io is SO_2, with H_2O the dominant species on the other three moons, the composition of the plasma is predominantly H^+,O^{+z}, S^{+z}, with a smaller component of undissociated, molecular ions (SO_2^+, SO^+, NaX^+, etc) found, primarily, close to Io, the principal source of the plasma. Although the flux of ions and electrons is not large by laboratory standards, the plasma energy flux to the surfaces or atmospheres of Europa and Io is larger than the solar UV flux [88].

An important issue for irradiation chemistry is the radiation dose vs. depth [88]. This is shown in Fig. 8 for Europa with the vertical axis the time required to achieve a dose of 100 eV per molecule in H_2O. This is a useful form since radiation chemists typical give yields as G-values. Geologist have suggested the youngest surface ages are $\lesssim 10^{6-7}$ years on Europa, during which time significant doses are acquired at all depths above $\sim$10 g/cm^2, Fig 9. Since over most of the surface the solar photon penetration depths are much smaller than this, the optical layer ($\sim$1 μm) is primarily altered by the incident plasma.

Because any H_2 produced in irradiated ice diffuses efficiently to the surface and is lost to the vacuum, the irradiated ice is permanently altered. Therefore, there is a depletion of H and formation of trapped O and OH, so the penetrated layer is oxidizing, as well as having an enhanced D/H ratio. These radicals can react directly: OH+OH $\rightarrow$ H_2O_2 and OH+O$\rightarrow$ HO_2. Reimann et al. [61] measured the fluence and temperature dependence for the production of O_2 from a thin ice sample in a vacuum exposed to energetic Ne^+. These ions were used to represent the energetic O^+ ions in the Jovian plasma. They found a correlation between the loss of H_2 and the production and loss of O_2. H_2 exhibited a prompt component followed by a gradually increasing component. The former comes from the surface and the latter depends on the film thickness for ions penetrating to the substrate. Reimann et al. noted an activation barrier 0.05-0.07eV and considered diffusion of the radicals produced. Sieger et al. [68] found similar results for incident electrons. They concluded that a non-diffusing precursor is first formed (cross section $\sim 10^{-18} cm^2$) and a subsequent electron produces the observed O_2 (cross section $\sim 10^{-16} cm^2$) in a temperature independent process. Therefore, trapped O as H_2O - O , H_2O-O + e $\rightarrow$ H_2 + O_2 is a candidate and they suggest that the activation energy may be associated molecular orientation changes. Alternatively, a hot O atom reacting with a trapped OH + O(hot)$\rightarrow$H + O_2 may be a candidate.

Since energetic ion and electron irradiation produces H_2 and O_2, we predicted that the Europa has a tenuous O_2 atmosphere [92]. That is, the H_2 desorbed would readily escape from a moon's gravitational field but the heavier O_2 would not. In addition, the O_2, unlike H_2O, does not condense at the surface temperatures on these moons, $\gtrsim$80K. Remarkably an O_2 atmosphere was indirectly observed by HST both on Europa and Ganymede . In a parallel set of discoveries, a reflectance band in the visible, similar to that for solid O_2 [91], was seen at low latitudes on Ganymede and, more recently, on Europa and Callisto. In addition, a likely radiation-induced UV feature associated with O_3 was seen on Ganymede [93] and subsequently on the icy satellites of Saturn.

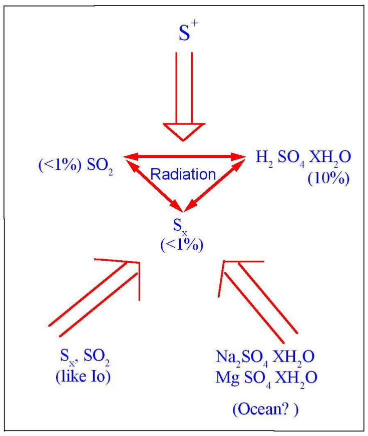

Figure 10. Sulfur cycle on Europa.

The recent observation of peroxide on Europa gave a clearly identifiable radiolytic product [94] This molecule, formed readily in the presence of a dilute sulfuric acid, may now be used as a kind of a dosimeter for surface radiation effects. Recently, Moore and Hudson[95] showed that at the temperatures relevant to Europa an electron scavenger (like sulfuric acid) is needed to accumulate sufficient peroxide making the comparison with more distant icy objects more interesting and, possibly, allowing us to extract compositional information.

The exciting observation that the hydrated mineral bands seen by [77] are primarily radiolytically-formed, frozen, dilute sulfuric acid [89] was supported by the laboratory data on radiolysis of frozen sulfur/water mixtures. Summarizing the available data, it was clear that the other radiolytic products, SO_2 and chain sulfur, are present. These are produced at the appropriate levels ($< 1\%$) to account for the visible reflectance in the chaos regions of Europa and the depth of Europa's SO bands. Therefore, we proposed that, in the surface layer penetrated by the energetic ions and electrons, a radiolytic sulfur/ice cycle (Fig. 10) is maintained, with sulfur being cycled, rapidly on a geologic time scale, among three forms, independent of the original source of the surface sulfur. Therefore, a separate indicator is needed to determine the source of S at Europa. There is sufficient sulfur implanted to account for the observations[74], however, in two recent papers [22, 96] it has been suggested that the radiolytic decomposition of $Na_2\ SO_4\ XH_2O \rightarrow Na + NaHSO_4\ (X\text{-}1)H_2O \rightarrow 2\ Na + H_2SO_4\ (X\text{-}2)H_2O$) could both initiate the sulfur cycle and produce the observed Na. Using this, the sodium observations at Europa were shown to be suggestive of an internal source of Na which apparently reaches the surface in the chaos areas, possibly salts or carbonates from Europa's underground ocean. CO_2 in ice is also seen, strengthening the picture that carbonates are being decomposed.

7.2 Sputtering of Saturn's E-ring Grains

The role of radiation bombardment of icy surfaces is even more spectacular in Saturn's inner magnetosphere. There the small, bright icy moons of Saturn (Mimas, Enceladus, Tethys, Dione and Rhea) are also irradiated by the trapped plasma, as are the grains in the largest planetary ring in the solar system, the diffuse E-ring [78]. Whereas radiolytic surface chemistry is the dominant feature of the Jovian satellites, for the lower temperatures of the icy Saturnian satellites, sputtering of H_2O dominates, with smaller amounts of O_2 and H_2.

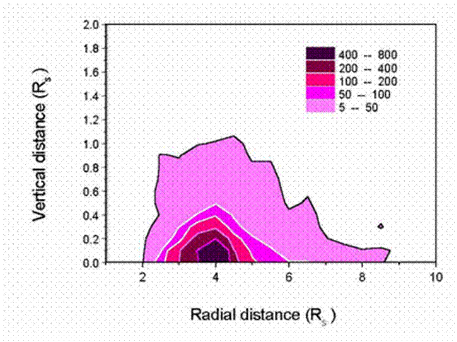

Figure 11. Neutral OH cloud for a large source at Enceladus.

The presence of a giant, toroidal atmosphere of sputter-produced water-ice products at Saturn. Remarkably, the OH component of that cloud was observed using Hubble Space Telescope. However, it was about thirty times more dense than predicted. In order to attempt to explain such densities we re-examined the sputtering of the icy surfaces, considering enhancements due to non-normal incidence, grain charging, and small grain size (discussed below), as well as a more careful extrapolation of the available data. We constructed the giant OH cloud by tracking the sputtered H_2O as it orbited Saturn, allowing for dissociation to form OH and then loss by ionization (Fig. 11). Using the best available data on the plasma and the most recent observations, we concluded that there must indeed be >10 times more surface available for sputtering than is seen optically, an exciting result. This is most likely in the form of freshly produced small grains associated with Saturn's E-ring, either from activity on Enceladus or due to collisions of small, as yet unseen, objects. Cassini will have on it a good time of flight mass spectrometer capable of detecting sputtered molecular species in the plasma, so that for the first time in the outer solar system a secondary ion mass spectrometry (SIMS) experiment of the surfaces will be carried out, of the type performed routinely in the laboratory.

8. Applications:Interstellar Medium

Dust in the interstellar medium (ISM) can exist in a variety of environments, from the hot intercloud medium to the cold neutral clouds. This dust contains most of the refractory material in the ISM and accounts for extinction, polarization, and scattering of light, as well as for certain absorption and emission features. The dust also plays an important role in determining the total energy balance, converting light to infrared emission and heating the clouds through photoelectron emission. It is estimated that $\sim 2/3$ of the grain mass in the ISM is tied up in grains with radius, a, less that $\sim 0.05\mu$m, accounting for the UV extinction, and $\sim 20\%$ in small grains, $a < 0.025\mu$m, which accounts for the steep rise in the UV extinction (see papers in this issue).

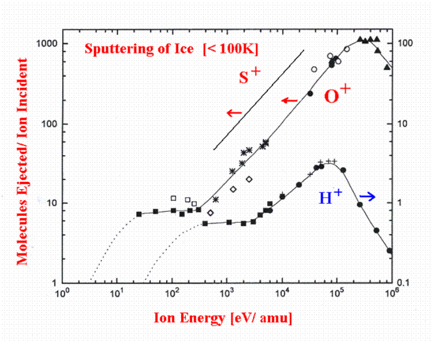

Figure 12. Sputtering yield of water ice from modified TRIM version (lines), calibrated to experimental data shown as symbols

However, this is not a static environment since grains are being eroded (sputtered) by the hot gas atoms or the local plasma, by grain-grain collisions, and either directly or indirectly by the cosmic ray ions. This loss competes with grain growth. Here we review the data on the sputtering of small refractory or icy grains in a hot plasma formed in a shocked region as well as the sputtering of the icy mantles of larger grains by cosmic rays ions in molecular clouds. In Table II was shown typical energies of H^+ and He^{+z} in interstellar shocks. We first describe the enhanced sputtering of small grains by a plasma in the threshold region and we then consider spike models used for calculating the grain erosion..

8.1 Enhanced Sputtering of Small Grains

In the sputtering of small grains edge effects are dominant. It has been shown that weakly attached surface components are readily eroded and that the enhancement due to angular incidence is always important. In addition, energetic particles can penetrate the grain and sputter at the exit surface. Since the tracking of the energetic recoils in the grain is required, we created a MC BCA code by modifying the TRIM program to track the incident ion and all of the recoils in a spherical grain. At the grain surface we applied sputtering data for those recoils crossing the surface 12. In this we first test the modified code for a flat surface and calibrated the surface effects to reproduce the available sputtering data in both the electronic and collisional regimes as a function of energetic particle energy and incident angle. This was done for the sputtering of carbon and low temperature water ice, for which the principal sputter products are C and H_2O respectively. In Fig. 12 we give the fit to the data given by this modified TRIM model for water ice over a broad range of energies and angles. This code was then applied to the spherical grain. It is seen in Fig. 13 that the enhancements in the yield can be significant [83].

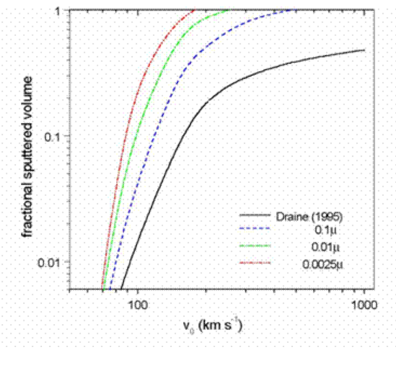

Figure 13. Fractional Sputtering yield from an interstellar shock with vellocity v_o for grains of radius $a = 0.1$, 0.01, and 0.0025 μm. The model from Draine [82] is also shown for comparisson.

8.2 "Spot heating" and "whole grain heating": TS Models

In the above, we neglected the total heat deposited, which is valid in many instances as both water and carbon are bound relatively tightly, but it clearly fails for very small grain size, large energy depositions and very volatile materials. Watson and Salpeter (WS) [84] proposed that small grains could be heated by incident cosmic ray (CR) bombardment. They evaluated the heating using a number of simplifying assumptions and calculated the evaporation rate of the grain material using a TS model. If heating and evaporation are localized in certain region of the grain they call it "spot heating", whereas if the energy deposited is spread nearly uniformly by the time sputtering occurs (as for small grains) they call it "whole grain heating". WS concluded that spot heating was negligible respect to whole grain heating because they consider only light CR ions. However, Léger, Jura and Omont (LJO) [85] showed that spot heating was dominant for volatile grains with radius $a > 0.25\mu$m by CR Fe bombarding a CO ice mantle. Using the CR abundances and energy spectrum they estimated the evaporation rate for a CO mantle to be 70 molec/$\left(cm^2 s\right)$. Their analysis, however, relied on a number of weak hypotheses.

a) A hot region of 20-200 Å in radius is rapidly created in the solid. This may not be true for the 0.2 GeV/amu Fe they study because the size of the region where ionizations are created is of the order of few hundred Å's, but there is only $\sim$1 ionizations/Å along the path of the ion. Therefore the track is not continuous, the excitations are dilute and act independently, creating small regions, much hotter than expected if the energy is distributed in the whole track.

b) The temperature profile is assumed to have a fixed shape: first a Gaussian and then a rectangular profile. Because evaporation depends exponentially on temperature (see flux formula, Eq. 10) this affects the estimate.

c) In the case of a small region where the energy density is such that the mean energy per molecule is larger than the binding energy of those molecules, analytic spike models do not work, as described above.

d) Finite size effects are neglected. The collision cascade may not be fully contained within the grain as discussed above. The large pressure propagates radially so when it reaches the surface of a large grain it may be weak, but for a small grain it may produce spallation from the side.

Hasegawa and Herbst (HH) [86] pointed out that the grain goes through heating and cooling cycles. Assuming the mean temperature during heating is T_{eff}, the evaporation rate $\langle k_i \rangle$ for species i is:

$$\langle k_i \rangle \approx F\,(T_{eff})\,k_i(T_{eff}, U_i) \approx 3.16\,10^{-19}\,k_i(70, U_i) = 3.16\,10^{-19}\,\nu_i \exp\left[-U_i/\left(k_B 70\right)\right] \tag{16}$$

They used $T_{eff} = 70$ K, and took the fraction of time the grain is hot as $F(T_{eff}) \approx t_{des}/t_{bombard}$, where t_{des} is the typical time for cooling due to desorbing species, $t_{des} \sim 10^{-5}$ s, and t_{des} is the typical time between CR bombardment by iron nuclei with sufficient dE/dx, $t_{des} \sim 3\ 10^{13}$ s. $\nu(T_{eff})$ is an average desorption rate which depends on the binding energy of the species. This approach is convenient since it gives a general expression for the desorption rate which is only a function of the binding energy of the absorbed species, and it has been used in several papers. However, the approximation used for evaporation has the same problems mentioned above.

After a heavy CR passes through a large grain the following occurs [87]:

1) $10^{-17} - 10^{-13}$ s. Energy is deposited in a region with a radius of the order of 100 Å and is rapidly distributed by secondary electrons and hot recoils.

2) $10^{-13} - 10^{-11}$ s. Sputtering occurs due to kinetic energy transport following energetic energy release events giving Y_{col}. "Temperature" is not well defined during this non-equilibrium stage, but the kinetic energy of atoms can reach 10^4 K and hot ejecta can take away ~20% of the deposited energy.

3) $10^{-11} - 10^{-9}$ s. Early thermal sputtering, $Y_{th-early}$, occurs following decay of the energetic recoil cascades and due to lower energy, energy-release events. This comes mainly from an extended radial region around the ion track. The temperature profile in the grain is not uniform and temperature near the track can be few hundred K. Ejecta are colder and take away ~5% of the deposited energy.

4) $10^{-9} - 10^{-5}$ s. Temperature in the grain is roughly uniform and decreases gradually due to evaporative cooling giving $Y_{th-late}$.

For a small grain, the temperature may already be roughly uniform by 10^{-10} s, but will still be higher than ~100 K. Due to size effects the energy taken away in step 2 is larger than 20%. Radiative cooling may be neglected compared to evaporative cooling in all these stages for grains of radius $a \ll 0.1\mu$m. The total sputtering yield is:

$$Y = Y_{col} + Y_{th-early} + Y_{th-late} \tag{17}$$

LJO neglect Y_{col} and treat $Y_{th-early}$ roughly. HH neglect both Y_{col} and $Y_{th-early}$. The key point is that late thermal ejection can occur over relatively long times, giving a large contribution to the yield. However, the first two contributions may be as important as or even dominate the last. Taking this into account gives results in the high energy density regime within factors 2-10 of the LJO or HH estimates. In a recent paper the results from MD calculations and the extrapolation of the available laboratory data were used estimate the fraction of CO and H_2O that will be seen in the gas phase in a low temperature molecular cloud due to desorption from grains by GeV CR-iron ions [87]. Fig. 14 shows snapshots from MD simulations of a grain hit by a cosmic ray. These simulations allow to calculate $(Y_{col} + Y_{th-early})$, while $Y_{th-late}$ can be calculated following simple evaporation models. Although a number of the approximations in LJO and HH were incorrect, the ratios of gas-phase to condensed phase CO did not change considerably due to cancellation of errors.

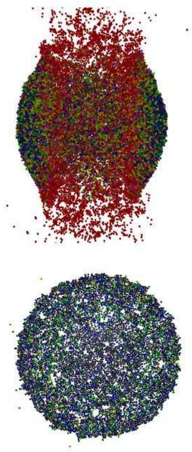

Figure 14. Snapshots from MD simulations of CR-induced sputtering from a "CO-like" grain of radius $a = 0.013\mu$m. Upper pannel shows heating with a track of 50 Åradius, and lower pannel shows whole grain heating. Only two central slices are shown, few ps after the bombardment. Both cases assume a total energy deposition of 8 keV, consistent with a Fe CR of ≈ 2 GeV.

9. Summary

Energetic ions, electrons and photons in many regions of our solar system, in young stellar objects and in the interstellar medium impact and modify the imbedded surfaces. This leads to sputtering (desorption) as well as chemical alteration of the surfaces. This has been shown to be critical for understanding the reflectance spectra of the Galilean satellites of Jupiter [74]. X-ray-induced desorption may maintain gas phase volatiles in young stellar objects [79], heavy cosmic-ray ions [87] and Lyman-α photons produced by cosmic rays protons may be responsible for maintaining the volatiles observed in the gas phase in cold molecular clouds, and energetic ions and electrons maintain a giant toroidal atmosphere in Saturn's inner magnetosphere 12.

In this chapter we briefly described the effect of radiation on materials in space. We primarily reviewed data for sputtering and, more importantly, the models needed to extrapolate that data or apply it to materials for which there is no data. It is important to remember that sputtering and the chemical changes induced in the material are intimately connected. First, reactions may be induced by implanted ions, as is the case for protons bombarding the lunar surface or sulfur ions bombarding Europa's surface. Second, the most volatile species in the material or the most volatile species formed by the radiation are preferentially ejected. This changes the composition of the material in the surface layer. This effect is striking demonstrated on Jupiter's moons. At Europa, oxygen, sodium and potassium atmospheres are maintained by decomposition of the surface [74] and at Callisto a CO_2 atmosphere is likely to be due to decomposition of organics in the surface [80, 81]. These surfaces have also been seen to contain trapped volatiles and refractory absorbing species produced by the radiation decomposition of the surface material. In the coming years, exciting spacecraft missions such as the Cassini mission and new space telescope data will considerably expand the observational data base. Understanding this data base will require a much better understanding of sputtering, radiolysis and photolysis for a much broader range of materials.

Acknowledgments

The work at Virginia was supported by the NSF Astronomy Divison and the Origins Program and NASA Headquarters. The work of E.M.B. was partially performed under the auspices of the U. S. Department of Energy by the University of California, Lawrence Livermore National Laboratory under Contract No. W-7405-Eng-48.

References

[1] W. M. Calvin, Planetary Report **XIX**, March/April 1999, pp. 8.

[2] Johnson, R.E. and J. Schou, in *Fundamental Processes in The Sputtering of Atoms and Molecules*, P. Sigmund ed., Mat-fys. Medd. Dan. Vid. Selsk **43**, Mem. Roy. Dan. Soc., Copenhagen, p. 403-494, 1993.

[3] A number of results, including movies of MD simulations can be found at: http://dirac.ms.virginia.edu/~emb3t/research/research.html.

[4] J. F. Ziegler, J. P. Biersack and U. Littmark, *The stopping and range of ions in solids*, Pergamon Press, New York, U.S.A, 1985.

[5] M. J. Berger and H. Paul, in IAEA-TECDOC-799, *Atomic and Molecular data for radiotherapy and radiation research*, IAEA, Vienna, 1995, pp. 415-546.

[6] O. B. Firsov, Zh. Eksp. Teor. Fiz. **33** (1957) 696, [Sov. Phys. JETP **6** (1958) 534].

[7] J. Lindhard, M. Scharff and H. E. Schiøtt, K. Dan. Vidensk. Selsk. Mat. Fys. Medd. **33** (1963) 14.

[8] F. Bloch, Z. Phys. **81** (1933) 363. Ann. Phys. **16** (1930) 285.

[9] H. A. Bethe, Ann. Phys. **5** (1930) 325.

[10] CASP, by G. Schiwietz and P.L. Grande is available at the web-site http://www.hmi.de/people/schiwietz/casp.html

[11] J. P. Biersack and L. G. Haggmark, Nucl. Instr. and Meth. **174** (1980) 257.

[12] TRIM was first developed by J. P. Biersack and and coworkers in 1980's. For instance see J. P. Biersack and W.D.Eckstein, Apply. Phys. A **34** (1984) 73. The latest version of "TRIM", SRIM 2000, can be downloaded for free in J. F. Ziegler's web site: http://www.srim.org/.

[13] P. Sigmund, Phys. Rev. **184** (1969) 383.

[14] E. M. Bringa and R. E. Johnson, Surface Science 451 (2000) 108.

[15] E. M. Bringa, R. E. Johnson and M. Jakas, Phys. Rev. B 60 (1999) 15107.

[16] H.G. Paretzke, D.T. Goodhead, I.G. Kaplan and M. Terrisol, in IAEA-TECDOC-799, *Atomic and Molecular data for radiotherapy and radiation research*, IAEA, Vienna, 1995, pp. 633-739.

[17] R. E. Johnson, in *Ionization of Solids by heavy particles*, R. A. Baragiola ed., Plenum Press, 1993, pp. 419-438.

[18] L. Sanche, T. D. Märk, and Y. Hatano, in IAEA-TECDOC-799, *Atomic and Molecular data for radiotherapy and radiation research*, IAEA, Vienna, 1995, pp. 277-330. Z. Herman, T. D. Märk, and L. Sanche, same book, pp. 371-414.

[19] V.Cobut, Y.Frongillo, J.P.Patau, T.Goulet, M.J.Frase, J.P.Jay-Gerin, Radiat. Phys. Chem. **51** (1998) 229. Y.Fongillo, T.Goulet, M.J.Fraser, V.Cobut, J.P.Patau, J.P. Jauy-Gerin, Radiat. Phys. Chem. **51** (1998) 245.

[20] A. I. Ryazanov, A. E. Volkov, S. Klaumünzer, Phys. Rev. B **51** (1995) 12107.

[21] P. Sigmund and C. Claussen, J. Appl. Phys. **52** (1981) 990.

[22] Johnson, R.E., Icarus 143,429-433 (2000).

[23] H. M. Urbassek and J. Michl, Nucl. Instr. and Meth. B **122** (1997) 427.

[24] C. Watson and T. Tombrello, Rad. Eff. **89** (1985) 263.

[25] L. E. Seiberling, J. E. Griffith, and T. A. Tombrello, Rad. Eff. **52** (1980) 201.

[26] R. E. Johnson and M. Liu, J. Chem. Phys. **104** (1996) 6041.

[27] M. W. Thompson, Philos. Mag. **18** (1968) 377.

[28] P. Sigmund, in *Sputtering by Particle Bombardment*, R. Behrish ed., Top. Appl. Phys. **47**, Springer, Heidelberg, 1981, p. 9.

[29] M. Toulemonde, Ch. Dufour, A. Meftah, and E. Paumier, presented at International Conference on Atomic Collisions in Solids, ICACS 18, Odense, Denmark 1999.

[30] R. H. Ritchie and C. Claussen, Nucl. Instr. and Meth. **198** (1982) 133.

[31] E. M. Bringa and R. E. Johnson, Phys. Rev. Lett. 88 (2002) 165501.

[32] H. Urbassek, Rad. Effects and Defects **142** (1997) 439 .

[33] E. M. Bringa, R. Papaleo and R. E. Johnson, Phys. Rev. B 65 (2002) 094113.

[34] R. E. Johnson and R. Evatt, Rad. Eff. **52** (1980) 187.

[35] M. Jakas, Rad. Effs. and Deffs. in Solids **152** (2000) 157.

[36] E. M. Bringa, R. E. Johnson and L. Dutkiewicz, Nuc. Inst. Met. B 152 (1999) 267.

[37] R. E. Johnson, J. de Physique C2 **50** (1989) 251.

[38] C. Claussen, Nucl. Instr. and Meth. **194** (1982) 567.

[39] D. Fenyö and R. E. Johnson, Phys. Rev. B **46** (1992) 5090.

[40] Johnson, R. E., Pirronello, V., Sundqvist, B.U.R., Donn, B., "Desorption of Large Molecules from Grains in Dense Clouds", Astrophys. J., 379 (1991) p. L75-L77.

[41] Jakas, M.M., Bringa, E.M., and Johnson, R.E. 2002, Phys. Rev. B 65, 165425

[42] W. D. Eckstein, *Computer Simulations of Ion-Solid interaction*, Springer-Verlag, Berlin, 1991.

[43] *Atomic & ion collision in solids and at surfaces*, R. Smith ed., Cambridge University Press, 1997.

[44] H. M. Urbassek, Nucl. Instr. and Meth. B **22** (1987) 480.

[45] M.H. Shapiro, Rad. Eff. and Defects in Solids **142** (1997) 259.

[46] M. Jakas and D. Harrison, Phys Rev. Lett. **55** (1985) 1782.

[47] M. T. Robinson's MARLOWE web page:
http://www.ssd.ornl.gov/Programs/MARLOWE/MARLOWE.html.

[48] P. Sigmund *et al.*, Nucl. Instr. and Meth. B **36** (1989) 110.

[49] M. P. Allen and D. J. Tildesley, *Computer Simulation of Liquids*, Clarendon Press, 1987.

[50] D. C. Rapaport, *The art of molecular dynamics simulation*, Cambridge Univ. Press, 1995.
http://www.cup.cam.ac.uk/onlinepubs/ArtMolecular/ArtMoleculartop.html

[51] MD primer by Furio Ercolesi, http://www.sissa.it/furio/md/md/md.html. HTML or Postcript format.

[52] Ł. Dutkiewicz, R. Pedrys, J. Schou, and K. Kremer, Europhysics Let. **27** (1994) 323. Ł. Dutkiewicz, R. Pedrys, and J. Schou, Nucl. Instr. and Meth. B **100** (1995) 217. Ł. Dutkiewicz, R. Pedrys, and J. Schou, Europhys. Lett. **36** (1996) 301.

[53] Z. Insepov, I. Yamada, Nucl. Instr. and Meth. B **121** (1997) 44.

[54] L.V.Zhigilei and B.J.Garrison, *Multiscale Modelling of Materials*, T. Diaz de la Rubia et al. eds., Mat. Res. Soc. Symp. Proc. **538** (1999) 491.

[55] F. F. Abraham, J. Broughton, N. Bernstein, and E. Kaxiras, Phys. Rev. B **60** (1999) 2391.

[56] Madey, T.E., R.E. Johnson and T.M. Orlando, "Far-out Surface Science: Radiation-Induced Surface Processes in the Solar System," Surf. Sci. 500, 838-858 (2002).

[57] G. Betz and K. Wien, Int. J. Mass Spec. and Ion Proc. **140** (1994) 1.

[58] R. L. Fleischer, P. B. Price, R. M. Walker, and E. L. Hubbard, Phys. Rev. **156** (1967) 353.

[59] D. Lesueur and A. Dunlop, Rad. Eff. and Def. in Solids **126** (1993) 163.

[60] R. Kelly, Nucl. Instr. and Meth. B **46** (1990) 441.

[61] C.T. Reimann *et al.*, Surf. Sci. **147** (1984) 227.

[62] R. Pedrys *et al.*, Nucl. Instr. and Meth. B **164-165** (2000) 861.

[63] L. Dutkiewickz, R. Pedrys, J. Schou and K. Kremer, Phys. Rev. Lett. **75** (1995) 1407.

[64] H. H. Andersen et al., Phys. Rev. Lett. **80** (1998) 5433.

[65] D. E. David and J. Michl, Prog. Sol. Stat. Chem. **19** (1989) 283.

[66] R. Pedrys, Nucl. Instr. and Meth. B **48** (1990) 525.

[67] H. G. Heide, Ultramicroscopy **14** (1984) 271.

[68] M. T. Sieger, W. C. Simpson, and T.M. Orlando, Phys Rev. B **56** (1997) 4925.

[69] W. L. Brown *et al.*, Nucl. Instr. and Meth. B **1** (1984) 307.

[70] K.M. Gibbs, W. L. Brown, R. E. Johnson, Phys. Rev. B **38** (1988) 11001.

[71] E. M. Bringa and R. E. Johnson, Nuc. Inst. Met. B 180 (2001) 99.

[72] Johnson, R.E. and T.I. Quickenden, J. Geophys. Res.102 (1997) 10985-10996.

[73] M. Famá, D. A. Bahr, B. D. Teolis and R. A. Baragiola, Nucl. Instr. Methods. Phys. Res. (submitted-published?)

[74] R. E. Johnson, R.W. Carlson, J. F. Cooper, C. Paranicas, M. H. Moore, M. Wong, In *Jupiter: Planet, Satellites & Magnetosphere*, ed. F. Bagenal, Univ. Arizona Press, Tucson, 2002).

[75] Khurana, K.K., et al., Nature 395, 777-780 (1998).

[76] Kivelson, M.G., et al, Nature 384 (1996) 537.

[77] McCord, T.B., et al., J. Geophys. Res. 104 (1999) 11827.

[78] Johnson, R. E., Pospieszalska, M. K., Sieveka, E. M., Cheng, A. F., Lanzerotti, L. J., and Sittler, E. C., Icarus 77 (1989) p. 311-329.

[79] Najita, Joan; Bergin, Edwin A.; Ullom, J. N., Astrophys. J., 561, (2001) 880.

[80] Carlson, R.W., Science 283, 820-821 (1999).

[81] Johnson, R.E., In Chemical Dynamics in Extreme Environments (R. Dessler, Ed), Adv. Ser. In Phys. Chem. World Scientific, Singapore, 11, Chap 8(2001) 390 .

[82] B. T. Draine, Astrophys. Space Sci. 233, 111 (1995)

[83] S. Jurac, R. E. Johnson, and B. Donn, Astrophys. J. 503, 247 (1998)

[84] Watson, W.D. and Salpeter, E.E. 1972, Astrophys. J. 334, 771

[85] Leger, A., Jura, M., and Omont, A. 1985, Astron. Astrophys. 144, 147

[86] Hasegawa,T., and Herbst, E. 1993, Mon. Not. R. Astron. Soc. 261, 83

[87] E.M. Bringa and R.E. Johnson, Astrophys. J., (2002) accepted. E. M. Bringa and R. E. Johnson, Nucl. Instr. and Meth. in Phys. Res. B 193/194 (2002) 370.

[88] Cooper, J.F., R.E. Johnson, B.H. Mauk, H.B. Garrett, and N. Gehrels, Icarus 149 (2001) 133.

[89] Carlson, R.W., R.E. Johnson and M.S. Anderson, Science 286 (1999) 97.

[90] Bagenal, F., J. Geophys. Res. 99 (1994)11043.

[91] Calvin, W. M., R. E. Johnson, and J. A. Spencer, Geophys. Res. Lett. 23(1996) 673.

[92] Johnson, R.E., Energetic Charged-Particle Interactions with Atmospheres and Surface, Springer-Verlag, Berlin (1990).

[93] Noll, K.S., R.E. Johnson, A.L. Lane, D.L. Dominigue, H.A. Weaver, Science 273, 341-343 (1996).

[94] Carlson, R. W., et al.. Science 283 (1999) 2062.

[95] Moore, M.H. and R.L. Hudson, Icarus 145, (2000) 282.

[96] Leblanc, F., R.E. Johnson and W.L. Brown, Icarus (2002) in press